Click Here for Full Article

Eastern tropical Pacific hydrologic changes during the past 27,000 years from D/H ratios in alkenones

Katharina Pahnke,[1,2] Julian P. Sachs,[1,3] Lloyd Keigwin,[4] Axel Timmermann,[5] and Shang-Ping Xie[5]

[1]   The tropical Pacific plays a central role in the climate system by providing large diabatic heating that drives the global atmospheric circulation. Quantifying the role of the tropics in late Pleistocene climate change has been hampered by the paucity of paleoclimate records from this region and the lack of realistic transient climate model simulations covering this period. Here we present records of hydrogen isotope ratios (δD) of alkenones from the Panama Basin off the Colombian coast that document hydrologic changes in equatorial South America and the eastern tropical Pacific over the past 27,000 years (a) and the past 3 centuries in detail. Comparison of alkenone δD values with instrumental records of precipitation over the past $\sim$100 a suggests that δD can be used as a hydrologic proxy. On long timescales our records indicate reduced rainfall during the last glacial period that can be explained by a southward shift of the mean position of the Intertropical Convergence Zone and an associated reduction of Pacific moisture transport into Colombia. Precipitation increases at $\sim$17 ka in concert with sea surface temperature (SST) cooling in the North Atlantic and the eastern tropical Pacific. A regional coupled model, forced by negative SST anomalies in the Caribbean, simulates an intensification of northeasterly trade winds across Central America, increased evaporative cooling, and a band of increased rainfall in the northeastern tropical Pacific. These results are consistent with the alkenone SST and δD reconstructions that suggest increasing precipitation and SST cooling at the time of Heinrich event 1.

1. Introduction

[2]   An ever increasing number of low-latitude paleoclimate records demonstrates that tropical climate underwent substantial temperature and precipitation changes on glacial-interglacial and millennial timescales [e.g., *Benway et al.*, 2006; *Haug et al.*, 2001; *Leduc et al.*, 2007; *Peterson et al.*, 2000; *Peterson and Haug*, 2006; *Wang et al.*, 2004]. Sea surface temperatures (SST) in the tropics were $2°-4°C$ colder during the last glacial maximum (LGM) than during the Holocene [*Koutavas et al.*, 2002; *Stott et al.*, 2002], while terrestrial records indicate air temperature changes of $5°-6°C$ [*Colinvaux et al.*, 1996; *Stute et al.*, 1995]. Precipitation was reduced and northeasterly winds stronger in the Northern Hemisphere tropics during the last glacial and the short-lived (10^2-10^3 years (a)) cold episodes in the North

Atlantic such as the Younger Dryas and Heinrich meltwater events (H events) [*Bush et al.*, 1992; *Haug et al.*, 2001; *Hooghiemstra and van der Hammen*, 1993; *Hughen et al.*, 1996; *Mora and Pratt*, 2001; *Peterson et al.*, 2000]. At the same time, the southern tropics experienced wetter conditions [*Maslin and Burns*, 2000; *Mayle et al.*, 2004; *Wang et al.*, 2004, 2006]. This precipitation pattern is consistent with meridional shifts of the Intertropical Convergence Zone (ITCZ).

[3]   Climate modeling evidence [e.g., *Stouffer et al.*, 2007; *Timmermann et al.*, 2005, 2007b; *Zhang and Delworth*, 2005] supports the notion that meltwater pulses in the northern North Atlantic can disrupt the large-scale Atlantic meridional overturning circulation (AMOC) by reducing surface density and deepwater formation. A weaker AMOC leads to a decrease of the poleward heat transport in the North Atlantic [*Stocker and Johnsen*, 2003] and a cooling of surface waters. This cooling enhances the trade wind circulation [*Chiang and Bitz*, 2005; *Krebs and Timmermann*, 2007] and increases evaporation, thereby spreading the cooling southward. The enhanced northeasterly trades and SST cooling in the tropical North Atlantic lead to a southward displacement of the Intertropical Convergence Zone, documented by instrumental observations [*Chiang*, 2005; *Xie and Carton*, 2004], and reflected in tropical paleoproxy records by precipitation changes. The southward shift of the ITCZ in the Atlantic has also been shown to play a key role in the recovery of the AMOC after a major shutdown [*Krebs and Timmermann*, 2007].

[1]Department of Earth, Atmospheric and Planetary Sciences, Massachusetts Institute of Technology, Cambridge, Massachusetts, USA.

[2]Now at Lamont-Doherty Earth Observatory, Earth Institute at Columbia University, Palisades, New York, USA.

[3]Now at School of Oceanography, University of Washington, Seattle, Washington, USA.

[4]Woods Hole Oceanographic Institution, Woods Hole, Massachusetts, USA.

[5]International Pacific Research Center, School of Ocean and Earth Science and Technology, University of Hawaii at Manoa, Honolulu, Hawaii, USA.
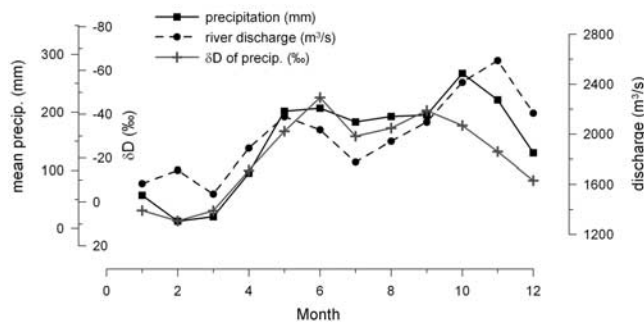
Figure 1. Annual changes in river discharge (M. T. Coe and N. Olejniczak, Center for Sustainability and the Global Environment (SAGE), Gaylord Nelson Institute for Environmental Studies, University of Wisconsin-Madison, Madison, Wisconsin, SAGE Global River Discharge Database, available at http://www.sage.wisc.edu/riverdata/, 1999), precipitation, and δD of precipitation in Panama (IAEA, ISOHIS database, 2006) (note inverted δD axis).

[4] Cooling in the Caribbean generates an anticyclonic surface circulation in the atmosphere, which spreads into the tropical North Pacific across Central America [*Timmermann et al.*, 2005, 2007b; *Zhang and Delworth*, 2005]. Over the tropical Pacific, enhanced northeasterly trade winds lead to enhanced Ekman pumping north of the equator, evaporative cooling, and a southward shift of the ITCZ. Because of positive air-sea coupling, the meridionally asymmetric SST, wind, and precipitation patterns can propagate into the western Pacific, thereby affecting salinity and rainfall in the Warm Pool [*Stott et al.*, 2004] and Australia [*Turney et al.*, 2004].

[5] On orbital timescales, two other important processes further contribute to the meridional position of the ITCZ. Orographic forcing of the glacial ice sheets over North America enhances the upper level stationary eddy momentum flux convergence at about 30°N, which leads to descending motion near 30°N and ascending motion around the equator. The resulting pressure gradient intensifies the northern trade wind circulation, which results in an enhancement of the oceanic subtropical cells, increased upwelling and colder sea surface conditions in the tropical and North Pacific [*Timmermann et al.*, 2004]. Furthermore, the seasonal cycle of clouds generates a meridional asymmetry of net annual mean shortwave radiation on precessional timescales [*Timmermann et al.*, 2007a]. The resulting heating asymmetry also affects the meridional position of the ITCZ considerably.

[6] While many paleoproxy and modeling studies have helped to elucidate the response of the Atlantic Ocean to orbital and millennial-scale forcing, the dynamics of the tropical Pacific on these timescales still remain elusive. While *Koutavas et al.* [2002] find a weak relative warming around Galapagos during Heinrich event 1, *Kienast et al.* [2006] reconstruct a cooling of 1.5°C with respect to mean late glacial SST at their northern tropical Pacific site. Many paleorecords from the northern tropics indicate drier conditions during the last glacial period compared to the

Holocene [e.g., *Haug et al.*, 2001; *Peterson et al.*, 2000]. However, two recent paleosalinity records show no change in salinity between LGM and Holocene [*Benway et al.*, 2006; *Leduc et al.*, 2007]. These seemingly conflicting results suggest that the patterns of orbital and millennial-scale climate change in the tropical Pacific need to be determined with more accuracy by using high-resolution proxy data as well as climate model simulations.

[7] To help synthesize the existing paleoproxy evidence for large-scale climate changes in the tropical Pacific during Termination 1, we present records of alkenone-derived SST and hydrogen isotope ratios in alkenones from the eastern tropical Pacific (5°N) for the past 27,000 a, and regional coupled modeling experiments that simulate the tropical Pacific response to an idealized cooling in the Caribbean, mimicking a Heinrich event.

[8] The paleodata document hydrologic changes in the Panama Basin and Colombia and provide evidence for cooling and increased rainfall during the last glacial-interglacial termination at ~17–13.5 ka, the time of Heinrich event 1 (H1).

2. Oceanography and Hydroclimatology of the Panama Basin

[9] Equatorial South America and the eastern tropical Pacific experience large precipitation changes in connection with the meridional migration of the ITCZ [*Xie et al.*, 2005], making the eastern tropical Pacific an ideal area to study linkages between low-latitude hydrologic changes and large-scale climate variations. In Panama and western Colombia, the seasonal precipitation pattern shows lowest rainfall in January to March and two maxima in May to June, and October to November. The rainfall maxima are interrupted by a short reduction during August and September: the midsummer drought (Figure 1). This pattern is the expression of the combined effects of the seasonal migration of the ITCZ and seasonal low-level wind jets that transport Pacific and Atlantic moisture into tropical South America [*Small et al.*, 2007]. Large rivers that drain the western flanks of the Colombian Andes transfer this precipitation signal to the Panama Basin, resulting in sea surface salinities (SSS) as low as 28 psu close to the coast [*Levitus et al.*, 1994] (Figure 2). The river San Juan in Colombia (average discharge: 2500 m³/s [*Restrepo and Kjerfve*, 2002]) constitutes the largest freshwater discharge to the Pacific from the Americas.

[10] In the western Colombian Andes, a westerly low-level wind jet, the Chocó Jet, causes large amounts of precipitation (6–13 m/a) making it one of the wettest places on earth [*Poveda and Mesa*, 2000]. The Chocó Jet is part of the southeasterly trade winds that cross the equator when the ITCZ is located in the Northern Hemisphere. Because of the Coriolis force, the winds become westerly and enter Colombia. The strength of the Chocó Jet is positively correlated with the meridional temperature gradient between the Niño 1 + 2 region (east Pacific cold-tongue area) and western Colombia (including the east Pacific off Colombia) [*Poveda and Mesa*, 2000; *Vernekar et al.*, 2003]. It thus contributes to the interannually varying positive (negative)
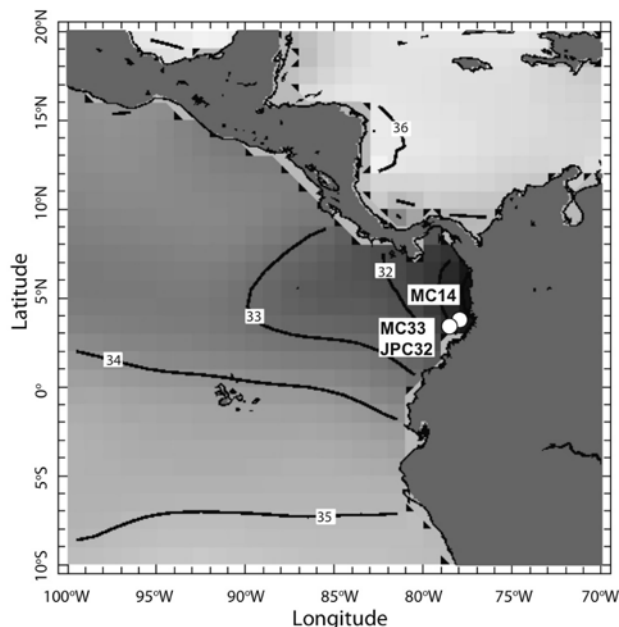
Figure 2. Core locations on a map of mean annual sea surface salinity [*Levitus et al.*, 1994].

rainfall anomalies in Colombia during cold (warm) ENSO phases when this temperature gradient is enhanced (reduced) [*Poveda and Mesa*, 1997; *Vernekar et al.*, 2003]. As the wind convergence of the ITCZ moves to the Southern Hemisphere where it reaches its southernmost position in February to March, the Chocó Jet ceases and precipitation in Colombia from south Pacific sources decreases substantially. Instead, the strengthened northeasterly trade winds enter the Panama Basin through a topographic gap in the Isthmus of Panama [*Chelton et al.*, 2000; *Xie et al.*, 2005]. This low-level Panama Jet forces the circulation in the Panama Basin to change from a prevailing anticyclonic circulation during summer to a cyclonic circulation from January to March [*Rodríguez-Rubio et al.*, 2003]. It further results in upwelling and surface cooling along a narrow strip extending from Panama southwestward [*Rodríguez-Rubio and Stuardo*, 2002]. Though precipitation in Panama and Colombia is at its annual minimum at that time (January–March), rainfall still reaches 440–480 mm/month in western Colombia (compared to annual maxima of 570–660 mm/month) (National Centers for Environmental Prediction/National Center for Atmospheric Research Reanalysis Project, see http://www.cdc.noaa.gov/cdc/reanalysis/index.html) (Figure 1), demonstrating the considerable amount of moisture transported from the Atlantic across the Isthmus by the Panama Jet.

3. D/H as Hydrologic Proxy

[11] The hydrogen isotopic ratio of water vapor (δD, expressed as deviation from Vienna Standard Mean Ocean Water, VSMOW, $\delta D = (D/H_{sample})/(D/H_{standard})-1) \times 1000$) is depleted in deuterium owing to the lower vapor pressure of DHO compared to H_2O [*Gat*, 1996]. Evaporation therefore leads to a relative D depletion of precipitation and D enrichment of lake water and seawater.

[12] The dominant control on δD values of precipitation in the tropics is the "amount effect": the inverse relationship between the isotopic ratio of precipitation and the amount of precipitation at a site [*Dansgaard*, 1964; *Rozanski et al.*, 1992]. Orographic lifting and long air mass trajectories further result in low δD values of precipitation, leading to rainfall δD values in western Colombia of $-25‰$ to $-89‰$ (long-term annual mean: $-57‰$) (Bogota, Colombia (International Atomic Energy Agency (IAEA), Isotopes in precipitation, Isotope Hydrology Information System (ISO-HIS) database, 2006, available at http://isohis.iaea.org, hereinafter referred to as IAEA, ISOHIS database, 2006)). Temperature-dependent fractionation, on the other hand, is close to zero at low latitudes [*Dansgaard*, 1964; *Gonfiantini et al.*, 2001; *Rozanski et al.*, 1992]. Changes in seawater δD values at low latitudes are therefore primarily controlled by changes in the amount of local precipitation and associated river runoff to the ocean.

[13] Algal lipids have been shown to be excellent recorders of water D/H ratios in culture and in the field [*Englebrecht and Sachs*, 2005; *Sachse et al.*, 2004, 2006; *Sauer et al.*, 2001; *Zhang and Sachs*, 2007]. Measuring the δD value of lipid biomarkers has several advantages over that of bulk organic matter, including the ability to ascribe them to individual groups or species and the stability of carbon-bound hydrogen to exchange with water on geologic timescales (at least for <1 Ma [*Sessions et al.*, 2004]).

[14] The δD value of long-chain alkenones ($C_{37:2-3}$) (δD_{alk}), produced by haptophyte algae (mainly the coccolithophorid species *Emiliania huxleyi* and *Gephyrocapsa oceanica*), has been shown to reflect the δD value of the water in which the alkenones were produced with near perfection ($R^2 > 0.99$) [*Englebrecht and Sachs*, 2005; *Paul*, 2002; *Schouten et al.*, 2006] (Figure 3). A negative offset of $\sim225‰$ is due to isotope fractionation during the synthesis of alkenones (initial deuterium depletion of the primary photosynthate of $\sim-171‰$ [*Yakir and DeNiro*, 1990] plus additional fractionation during biosynthesis). This suggests that δD values measured in alkenones from marine sediments can be used to reconstruct past changes in freshwater supply to the ocean and hence precipitation and river runoff.

[15] Two uncertainties with this approach are the potentially varying amounts of D/H fractionation during alkenone biosynthesis by different species or genera, and as yet unknown or poorly constrained environmental influences on D/H fractionation in alkenones [*Paul*, 2002; *Schouten et al.*, 2006; *Zhang and Sachs*, 2007]. If a succession of alkenone-producing species (or genera) occurs through time at a site, and different species discriminate against deuterium to varying degrees during alkenone biosynthesis, then a down core change in δD_{alk} values could arise in the absence of any change in water δD values. A similar case could be made for a change in light, nutrients, SST, SSS, etc., if any of those factors influence D/H fractionation during lipid synthesis.

[16] To date little is known about the dependence of D/H fractionation in alkenones (or any other lipid) on species or
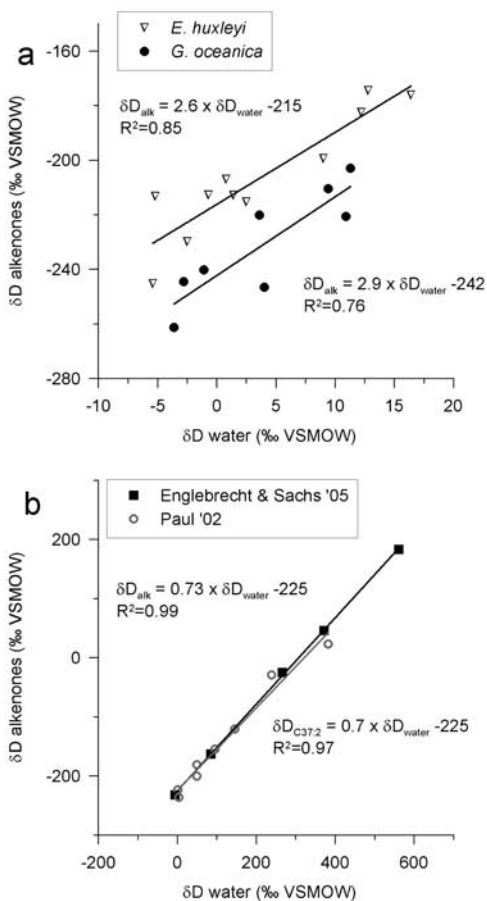
Figure 3. Alkenone δD versus water δD of culture studies. (a) δD_{alk} versus δD_{water} for *E. huxleyi* and *G. oceanica* [*Schouten et al.*, 2006]. (b) Same as in Figure 3a but culture data from *Englebrecht and Sachs* [2005] (squares) and *Paul* [2002] (circles) for *E. huxleyi*.

environmental conditions. *Schouten et al.* [2006] reported δD_{alk} values in *G. oceanica* that were $\sim 30\permil$ lower than in *E. huxleyi* grown in batch cultures (Figure 3). In the same experiments, a positive correlation of isotope fractionation with salinity, amounting to $\sim 3\permil$/salinity unit, was observed for both species, as was a negative correlation of D/H fractionation and growth rate. Conversely, no effect of growth rate on D/H fractionation in alkenones was observed by *Paul* [2002]. Moreover, results from chemostat (i.e., continuous culture) experiments with a marine diatom indicated no impact of growth rate on D/H fractionation in fatty acids [*Zhang and Sachs*, 2007]. Last, temperature changes had no effect on alkenone D/H fractionation in coccolithophorid batch cultures [*Schouten et al.*, 2006], but had a slight influence on D/H fractionation in lipids from green algal cultures [*Zhang and Sachs*, 2007].

[17] At present, the largest influences on D/H fractionation during alkenone biosynthesis appear to be the species producing the alkenones and the salinity of the water. However, as discussed below (section 5), species changes are unlikely to mask our δD_{alk} record, and salinity-dependent isotope fractionation would amplify the δD_{alk} signal

that is due to changes in the amount of precipitation and runoff to the Panama Basin. Other proxy data such as nannofossil abundances and $\delta^{18}O$ values of planktonic foraminifera are expected to elucidate these issues when they become available.

4. Material and Methods

4.1. Core Locations

[18] For the first down core study of alkenone δD values we chose three cores from the Panama Basin in the tropical eastern Pacific that were obtained during R/V *Knorr* cruise 176-2 in February–March 2004 (see http://www.marine.whoi.edu/kn_synop.nsf) (Figure 2). We sampled two short multicores, MC14 (4°50.81′N, 77°36.85′W, 884 m water depth, 32 cm long) and MC33 (4°39.99′N, 77°57.80′W, 2200 m water depth, 36 cm long), and the upper 800 cm of jumbo piston core JPC32 (same location as MC33). The core sites are located off of western Colombia, close to the mouth of the Rio San Juan. Given the salinity at our core site of 28.6 to 32.2 psu and an open ocean salinity of 34–34.5 psu [*Levitus et al.*, 1994], a simple concentration calculation suggests a freshwater contribution to the core site of 6–20.5%. The cores are therefore ideally located to sensitively monitor changes in river runoff and precipitation in the Colombian Andes, and to highlight their potential for a first test of the applicability of alkenone δD as hydrographic proxy. The proximity of the short cores to each other also permits testing the reproducibility of the δD signal recorded by alkenones.

4.2. Alkenone Purification for D/H Analysis

[19] Multicores MC14 and MC33 were sampled at 1 or 2 cm and 1 to 4 cm intervals, respectively. Core JPC32 was sampled every 10 cm in the upper 8 m. Lipids were extracted from the freeze-dried sediment samples (3–9 g) with dichloromethane (DCM) at 100°C and 1000 psi on a Dionex ASE-200 pressurized fluid extractor ($2\times$) and the total lipid extracts were combined and dried under a stream of N_2. Alkenone purification followed the protocol of *Englebrecht and Sachs* [2005] with slight modifications. Briefly, dry total lipid extracts were redissolved and hydrolyzed with 1N KOH in methanol:deionized water (3:1) at 60°C over night. Alkenones were extracted with 20 mL hexane ($3\times$), back extracted ($1\times$), dehydrated over Na_2SO_4 and dried under a N_2 stream. The extracts were redissolved in a minimum amount of hexane and applied to a 9 inch Pasteur pipette containing 5 cm of activated silica gel (100–200 mesh). The samples were eluted with hexane (hydrocarbons), DCM:hexane (1:1) (alkenones), and methanol (polar compounds). Further purification was achieved by argentation column chromatography using a 9 inch pipette containing silver nitrate-coated silica gel and eluting the alkenones in ethyl ether. A final purification of alkenones was performed using a 9 inch pipette filled with 4 cm of activated silica gel (100–200 mesh) and eluting with DCM:hexane (1:1). When necessary, branched and cyclic molecules were removed from the alkenone fraction through urea adduction.

[20] Alkenone purity, concentration and the relative abundance of $C_{37:3}$ and $C_{37:2}$ alkenones for SST estimation (see

below) were measured on 5% aliquots of each sample using an Agilent 6890N gas chromatograph with a Chrompack CP-Sil-5 column (60 m by 0.32 mm ID, 0.25 μm film thickness) and a programmable temperature vaporization inlet in solvent-vent mode. Helium was used as a carrier gas at a constant flow rate of 1.6 mL/min and compounds were detected by flame ionization. The oven was programmed from 110°C to 270°C at 40°C/min followed by a temperature increase of 2°C/min to 320°C, and an 18 min isothermal period. Alkenones were quantified using coinjected n-hexatriacontane (n-C_{36}) as a quantitation standard. The samples contained a series of $C_{37}-C_{39}$ alkenones and showed a clean baseline in a large area around the alkenones where internal standards were introduced later for hydrogen isotope analysis. C_{37}-alkenone concentrations ranged from 0.15 to 1.7 μg/g dry sediment, which yielded 3 to 13 μg (average: 3.4 μg) of C_{37} alkenones per sediment sample.

4.3. Hydrogen Isotope Analysis

[21] Hydrogen isotope ratios were determined by isotope ratio–monitoring gas chromatography mass spectrometry (irmGC-MS) on a ThermoFinnigan Delta[plus] XP equipped with a Trace GC and Combustion III interface, using methods adapted from *Sessions et al.* [1999] and *Sauer et al.* [2001]. The Trace GC was equipped with a PTV inlet operated in splitless mode, a 30 m DB-5 capillary column with 0.25 mm ID and 0.25 μm film thickness. With helium as carrier gas, the effluent from the GC entered the Combustion III interface, a graphite-lined tube held at 1400°C, where the sample was quantitatively pyrolyzed to graphite, H_2 and CO [*Burgoyne and Hayes*, 1998]. The hydrogen gas was then introduced to the mass spectrometer through an open split.

[22] A correction factor for H_3^+ ions formed in the source was determined daily by measuring the (m/z 3)/(m/z 2) response of ten different concentrations of H_2 reference gas [*Sessions et al.*, 2001]. A low and stable value of 3–4 was typically achieved. The sensitivity of the instrument was monitored by injection of four pulses of H_2 reference gas at the beginning and two at the end of each run.

[23] Two n-alkanes, nC_{36} and nC_{44}, with known δD values that bracket the alkenone peaks in the chromatogram, were coinjected with each sample and used as isotopic standards for the computation of alkenone δD with IsoDat 2.0 software (ThermoFinnigan) (all isotope standards were obtained from A. Schimmelmann of the Biogeochemical Laboratories, Indiana University, Bloomington, Indiana, United States). For each measurement, ~1 μg $C_{37:2+3}$ alkenones were injected in 1 μL to obtain intensities of ~1000 mV, at which the results were most reproducible. Samples were run in duplicate or triplicate, alkenone concentrations permitting, with a typical standard deviation of less than 5‰. An isotope standard was measured after every 7–10 samples to ensure accuracy of alkenone δD values. The standard contained a series of 15 homologous n-alkanes (nC_{16} to nC_{30}, mixture "Arndt-B"), with known δD values spanning a fivefold range in concentration and 214‰ in δD. The precision of δD measurements of this standard expressed as the average standard deviation of all measurements was ±3.7‰ (n = 79 injections) and the root-mean-

square (RMS) error was 4‰ (n = 1027 measurements). All δD results are reported with reference to the VSMOW standard.

4.4. Alkenone SST Estimation

[24] We estimated sea surface temperatures (SST) from the unsaturation ratio of $C_{37:3}$ and $C_{37:2}$ alkenones using the $U_{37}^{K'}$ index ($U_{37}^{K'} = C_{37:2}/(C_{37:2} + C_{37:3})$), and the empirically derived $U_{37}^{K'}$-SST equation of *Prahl et al.* [1988] ($U_{37}^{K'} = 0.034T + 0.039$). This culture-based equation has been corroborated by an extensive field study of globally distributed core top sediments [*Conte et al.*, 2006; *Müller et al.*, 1998] (600 core tops).

4.5. Stable Oxygen Isotopes

[25] Hispid and smooth-shelled species of the benthic foraminifera *Uvigerina* were picked from the fraction >250 μm of core JPC32 for stable oxygen and carbon isotope analysis. Most of the analyses were performed on individual specimens. In the upper 400 cm of the core sample spacing was 20 cm. Below that depth it was 40 cm. Analyses were carried out on a VG Prism mass spectrometer at the NOSAMS facility at Woods Hole Oceanographic Institution. Precision was better than 0.10‰ over the period of analyses as checked by routine runs of the NBS19 and other standards.

4.6. Age Models
4.6.1. Age Models for Multicores MC14 and MC33

[26] Age models for multicores MC14 and MC33 are based on ^{210}Pb dating. Seven to ten grams of dry sediment from the upper 20 cm and 14 cm of cores MC14 and MC33, respectively, were analyzed for ^{210}Pb on the gamma counter (Series 40 MCA, model GL2020) of the Department of Civil and Environmental Engineering at the Massachusetts Institute of Technology.

[27] The decay of atmospherically produced ^{210}Pb (excess or unsupported ^{210}Pb, $^{210}Pb_{exs}$), measured in marine or lacustrine sediments, provides a measure for the rate of sedimentation and can be used to derive an age-depth correlation for sediment sequences over the past ~150 a. The total amount of ^{210}Pb ($^{210}Pb_{total}$) in sediments has to be corrected for (supported) ^{210}Pb supplied through the decay of ^{226}Ra in the sediment. This was done by measuring the activity of ^{214}Pb and subtracting it from $^{210}Pb_{total}$. Age scales were then derived using the Constant Initial Concentration (CIC) model that assumes constant sedimentation rates and a zero age at the surface [*Goldberg*, 1963; *Krishnaswamy et al.*, 1971; *Turner and Delorme*, 1996].

[28] The $^{210}Pb_{exs}$ depth profiles of both cores (MC14, MC33) are shown in Figure 4a. Extrapolation of the age scales to the bottom of the cores at 32 cm (MC14) and 36 cm (MC33) indicates that MC14 spans the period from 1700 A.D. to the present and MC33 spans the period from 1600 A.D. to the present.

4.6.2. Age Model for JPC32

[29] The age model for core JPC32 is based on visual alignment of the benthic foraminiferal $\delta^{18}O$ record from core JPC32 with the global $\delta^{18}O$ stack of *Lisiecki and Raymo* [2005] (Figure 4b). According to this age model, the bottom of the studied section of JPC32 reaches 27 ka and
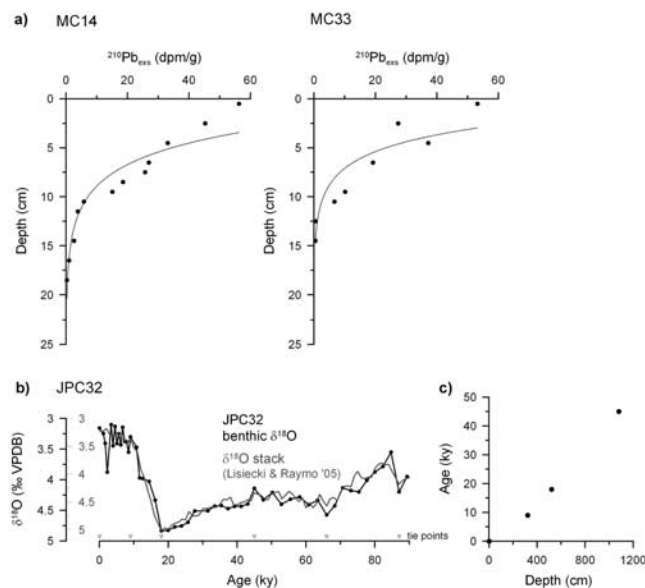
Figure 4. Age models for the multicores (MC14 and MC33) and JPC32. (a) The ^{210}Pb profiles for MC14 and MC33. (b) Benthic foraminiferal (*Uvigerina*) δ^{18}O record of core JPC32 over the past 90 ka compared with the global benthic δ^{18}O stack of *Lisiecki and Raymo* [2005]. Arrows mark tie points used to align the benthic record of JPC32 to the global δ^{18}O stack. (c) Age-depth plot for JPC32.

our sampling interval of 10 cm corresponds to a mean temporal resolution of 380 a.

[30] Accumulation rates for alkenone fluxes were calculated using dry bulk densities along the core.

5. Results and Discussion

5.1. Proof of Concept: Alkenone D/H Changes Over the Past 400 a

[31] Alkenone-derived SST estimates along MC14 and MC33 (Figure 5a) varied between 26.5 to 27.3°C and 26.3 to 27.2°C, respectively (Figure 5). The core top SST estimates of 27°C (MC14) and 26.7°C (MC33) are consistent with the mean annual atlas SST at the core sites of 26.9°C [*Levitus and Boyer*, 1994]. The most notable features in the SST records are small declines in temperature (~0.4°C) at around 1822 A.D. (MC14) and 1867 A.D. (MC33), relatively constant SSTs subsequent to that drop and a temperature increase by some 0.7°C at 1897 AD (MC14) and at 1922 A.D. (MC33). Subsequently, temperatures in MC14 remained around 27.2°C until the present but dropped to 26.5°C in MC33 and remained slightly lower than in MC14.

[32] Alkenone δD along cores MC14 and MC33, spanning the past three and four centuries, respectively, varied from −190 to −221‰ (MC14) and −195 to 219‰ (MC33) (Figure 5c). Prior to ~1900 A.D. both records show relatively similar values varying around a mean of −208‰ in core MC33 and slightly lower, around −210‰, in core MC14. After ~1900 A.D. the records diverge: while δD$_{alk}$ values in MC14 decreased, reaching

−221‰ at 1940 A.D., then increased again to a maximum value of −205‰ at 1988 A.D., δD$_{alk}$ values in core MC33 increased gradually to a maximum of −195‰ at 1986 A.D. Both records decrease in the 1990s to core top values of −220‰ (MC14) and −205‰ (MC33), respectively (Figure 5d). Superimposed on these general trends are shorter-duration changes in both records that show obvious covariations since ~1900. Two δD$_{alk}$ minima around 1940 and 1965 A.D. are followed by clear maxima around 1950 and 1986/1987 A.D., and δD$_{alk}$ decreases of −10‰ (MC33) and −15‰ (MC14) since the late 1980s. Though the first two of these short-term minima in core MC33 are within the error of measurement, they are significant in the more highly resolved core MC14 and are supported by several data points.

[33] The δD$_{alk}$ records in MC14 and MC33 show similarities in absolute value, amplitude and timing of changes (Figures 5c and 5d). The consistently lower δD$_{alk}$ values in core MC14 compared to MC33 are expected from the closer proximity of that site to the large freshwater source of the San Juan River. Indeed, the surface salinity measured at the site of MC14 was 0.9 psu lower than at the site of MC33 in February 2004 (29.4 psu versus. 30.3 psu). Higher δD$_{alk}$ values in core MC33, on the other hand, are consistent with its location further offshore under a stronger influence of more saline, less D-depleted open-ocean surface waters.

[34] In order to validate alkenone δD values in Colombian margin sediments as a hydrologic indicator, we compare our δD$_{alk}$ records to measured river discharge of Rio San Juan (Global Runoff Data Centre, Koblenz, Germany, see http://grdc.bafg.de) and precipitation at a nearby site in Panama (Barro Colorado Island 9.17°N 79.84°W (Smithsonian Tropical Research Institute, Balboa, Republic of Panama, see http://striweb.si.edu/esp)) (Figure 5b). (Unfortunately, records from Colombia only cover the period 1950–1985.) Both δD$_{alk}$ records clearly covary with each other since 1920 A.D. (r^2 = 0.73, n = 7) and with precipitation in Panama over the time period of overlap (MC33: r^2 = 0.76, n = 7; MC14: r^2 = 0.3, n = 8. The 5pt moving average of the precipitation record was taken and sampled at the sample spacing of the MC records). For example, the gradual decrease in rainfall and river discharge prior to 1990 A.D. is accompanied by an increase in δD$_{alk}$ values, and the recent precipitation increase in Panama is reflected in our records by a δD$_{alk}$ decrease. Small inconsistencies between the δD$_{alk}$ records and precipitation changes in Panama are likely because of uncertainties in the age models of our cores. These results support the use of δD$_{alk}$ as a proxy for past changes in freshwater supply to the ocean and allow us to interpret δD$_{alk}$ changes in the Panama Basin in terms of hydrologic variations in tropical South America.

[35] The δD$_{alk}$ divergence of our records at ~1900 A.D. indicates a salinity decrease at the inshore site of core MC14, and a trend toward higher salinity at the offshore site of core MC33 (Figure 5d). Core MC14 is located closer to the freshwater source of the San Juan and is likely to be more sensitive to changes in runoff and precipitation in Colombia than the more distal site of core MC33. An increase in precipitation and river discharge from the western Colombian Andes may have resulted from a north-
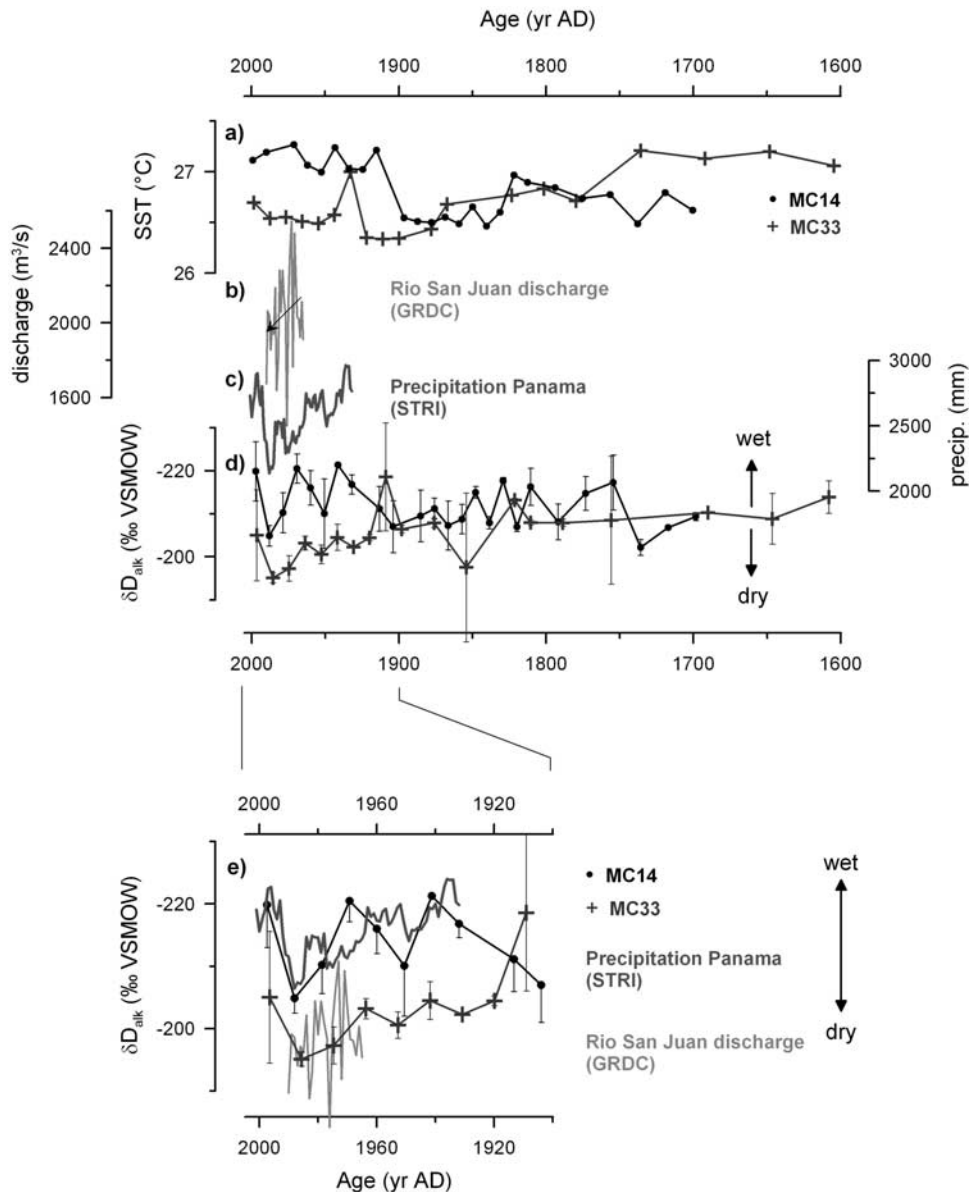
Figure 5. $U_{37}^{K'}$-derived SST and δD_{alk} records of multicores MC14 (circles) and MC33 (crosses). (a) SST and (d) δD_{alk} records over the past 300 and 400 a compared to (b) mean annual discharge of Rio San Juan (Global Runoff Data Centre, Koblenz, Germany, see http://grdc.bafg.de) and (c) an instrumental record of precipitation in Panama (seven-point running mean) (Smithsonian Tropical Research Institute, Balboa, Republic of Panama, see http://striweb.si.edu/esp). (e) Detailed view of the past ~100 a that are covered by the precipitation and discharge records (note inverted δD axes).

ward shift of the mean position of the ITCZ and/or a strengthening of the westerly Chocó Jet, presumably in association with increased meridional temperature gradients [*Poveda and Mesa*, 2000; *Poveda et al.*, 2001; *Restrepo and Kjerfve*, 2000].

5.2. Hydrologic and Sea Surface Temperature Changes Over the Past 27,000 a

5.2.1. Glacial-Interglacial and Holocene Changes

[36] $U_{37}^{K'}$-SST values in core JPC32 averaged ca. 25°C during the LGM (18–23 ka) and recorded 26.5°C during the late Holocene (0–5 ka) (Figure 6c). The core top SST of 27°C is in agreement with average $U_{37}^{K'}$ SSTs in the multicores of 26.8°C over the past 200 a and with the mean annual atlas SST at the core site of 26.9°C [*Levitus and Boyer*, 1994]. The mean glacial-interglacial SST change of ~1.3°C is within the range of amplitudes of 1.2°–3°C previously reported for this time interval in the eastern tropical Pacific [*Benway et al.*, 2006; *Kienast et al.*, 2006; *Koutavas et al.*, 2002; *Lea et al.*, 2000; *Leduc et al.*, 2007].

[37] The mid-Holocene (7 ka) to present period is characterized by a trend of increasing SST of 1°C. This
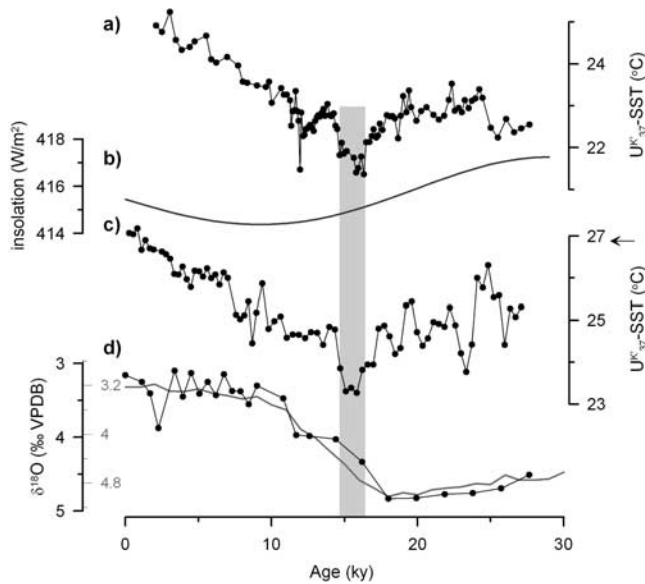
Figure 6. (a) Alkenone-derived ($U_{37}^{K'}$) sea surface temperature record from the eastern tropical Pacific (0°N) [*Kienast et al.*, 2006]. (b) Mean annual insolation at 5°N. (c) $U_{37}^{K'}$-SST record from Panama Basin core KNR176-JPC32 (5°N). (d) Benthic foraminiferal (*Uvigerina*) $\delta^{18}O$ record and the global benthic $\delta^{18}O$ stack of *Lisiecki and Raymo* [2005]. Shaded bar marks the early deglacial SST cooling that coincides with Heinrich event H1.

temperature increase is emerging as a tropical Pacific-wide feature that is documented in a growing number of, mainly alkenone-derived, SST records in the northern and southern tropics of the East and West Pacific [*Kienast et al.*, 2001; *Kienast et al.*, 2006; *Koutavas et al.*, 2002; *Koutavas and Lynch-Stieglitz*, 2003; *Koutavas et al.*, 2004; *Leduc et al.*, 2007]. The orbital precession pattern found in many tropical climate records [e.g., *Baker et al.*, 2001a; *Bush et al.*, 2002; *Cruz et al.*, 2005] cannot explain this Holocene SST feature since it appears in both hemispheres while precession imposes an opposite effect on insolation in the Northern and Southern Hemisphere. The temperature increase, however, coincides with an upward trend in annual mean insolation at midlatitudes to low latitudes (Figure 6). Studies of marine core tops and sediment traps demonstrate that alkenones, despite significant differences in seasonal and interannual alkenone export, record mean annual SST [*Conte et al.*, 2006; *Müller et al.*, 1998; *Prahl et al.*, 2005]. It is therefore plausible that mean annual insolation changes may be imprinted on midlatitude to low latitude SSTs as has previously been suggested for the time interval 47–23 ka [*Pahnke and Sachs*, 2006]. The amplitude of these insolation changes is small (~3.2 W/m² at 5°N) relative to insolation changes at high latitudes. However, low to midlatitude warming may be reinforced by local greenhouse effects caused by increased water vapor and cloud formation over warm ocean areas [*Hall and Manabe*, 2000]. It is also instructive to consider that 3.5–4 W/m² is the radiative increase accompanying a doubling of present

atmospheric CO_2 levels [*Ramaswamy and Members of IPCC Working Group I*, 2001], which is expected to cause global warming of 1.5°–4.5°C.

[38] Hydrogen isotope ratios measured on alkenones in core JPC32 varied between −222‰ and −183‰ (Figure 7b). The long-term trend over the past 27 ka indicates high δD_{alk} values during the last glacial period and lower δD_{alk} values during the Holocene. The core top value of −204‰ is consistent with the δD_{alk} value in multicore MC33 at the same location that averaged −205‰ over the past 200 a. The mean glacial to late Holocene δD_{alk} difference of 19‰ leaves an amplitude of ~11‰ after subtraction of glacial mean ocean D enrichment of ~8‰, owing to isotopicallly depleted ice on the continents (Figure 7). Given a higher glacial mean ocean salinity of ~+1 [*Duplessy et al.*, 1991] and the apparent salinity effect on alkenone D/H fractionation of ~3‰/salinity unit [*Schouten et al.*, 2006], our data suggest 8‰ higher glacial δD_{alk} values, presumably the result of diminished runoff. This is supported by the planktonic foraminiferal (*Globigerina bulloides*) stable oxygen isotope ($\delta^{18}O_{plk}$) record along our core that shows a glacial $\delta^{18}O$ enrichment of some 1.8‰ (LGM−late Holocene, Figure 7). Correction for local SST using the $U_{37}^{K'}$-SST estimates along JPC32 and global seawater $\delta^{18}O$ [*Schrag et al.*, 2002; *Waelbroeck et al.*, 2002] suggests a glacial local seawater $\delta^{18}O$ ($\delta^{18}O_{sw}$) enrichment of ~+0.8‰. We are aware that combining proxies from two different proxy carriers to correct $\delta^{18}O_{plk}$ for local SST changes (alkenones, produced by coccolithophorids, and planktonic foraminifera) is not ideal and we therefore refrain from interpreting short-term $\delta^{18}O_{sw}$ changes. However, the glacial-interglacial $\delta^{18}O_{sw}$ change of ~0.8‰ is substantial and cannot be entirely due to this shortcoming. The $\delta^{18}O_{plk}$ evidence therefore supports the glacial-interglacial change in surface water isotopic composition suggested by δD_{alk}. Given the linear relation of $\delta^{18}O$ and δD (meteoric water line [*Rozanski et al.*, 1993]), the observed glacial-interglacial $\delta^{18}O_{sw}$ change of ~0.8‰ should correspond to a δD change of 6.5‰. This is close to our estimated glacial-interglacial δD amplitude of 8‰ and thus further supports the reliable reflection of surface water isotopic changes in alkenones.

[39] *Schouten et al.*'s [2006] culturing studies indicated that *G. oceanica* produced alkenones that were about 30‰ more depleted in deuterium relative to *E. huxleyi* (Figure 3a). Changes in the abundance of *G. oceanica* relative to *E. huxleyi* were quantified by *Martínez et al.* [2006] in Ocean Drilling Program core 677B from 1.2°N in the Panama Basin (i.e., 3.2° of latitude south of our core site). During the LGM, *G. oceanica* abundances in core 677B were ~200% that of *E. huxleyi* abundances, while in the Holocene they dropped to ~50% [*Martínez et al.*, 2006] (Figure 8). The change in the relative abundance of the two species, absent any change in water δD, ought to have made LGM alkenones more depleted in deuterium relative to Holocene alkenones, the opposite of what we observe (Figure 8). Moreover, total alkenone concentrations and alkenone accumulation rates (calculated using dry bulk density) in JPC32, indicators of total coccolithophorid production, are consistently higher during the last glacial period compared to the Holocene (Figure 8). That is, if the
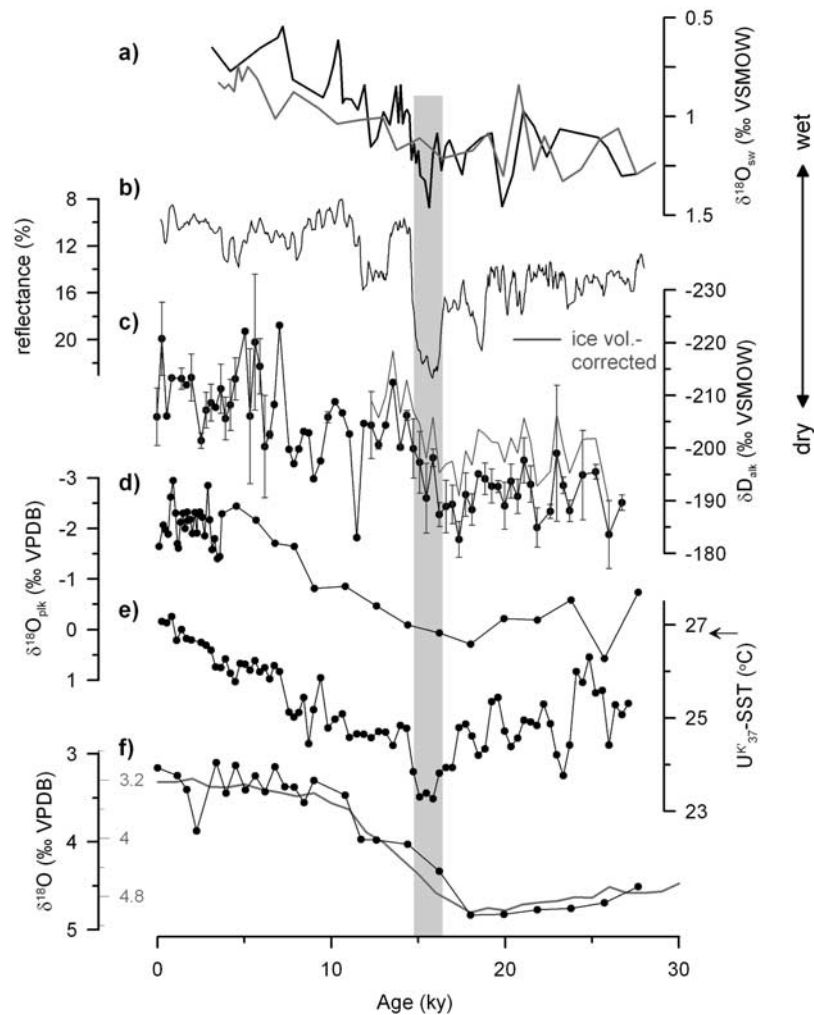
Figure 7. Paleorecords along core JPC32 compared to $\delta^{18}O_{sw}$ records from the Caribbean and the Cariaco Basin reflectance record. (a) $\delta^{18}O_{sw}$ records from the Caribbean (Ocean Drilling Program (ODP) Site 999A (shaded) and VM28-122 (solid) (corrected for global ice volume changes using the work of *Waelbroeck et al.* [2002]) that reflect changes in surface water salinity and thus precipitation [*Schmidt et al.*, 2004]. (b) Reflectance record from the Cariaco Basin (ODP Site 1002) indicating changes in precipitation and runoff [*Peterson et al.*, 2000]. (c) δD_{alk} record along core JPC32 (solid). Shaded curve is δD_{alk} corrected for mean ocean δD changes (using the mean ocean $\delta^{18}O$ curve of *Waelbroeck et al.* [2002] converted to δD using $\delta D = \delta^{18}O*8.13 + 10.8$ [*Rozanski et al.*, 1993]). (Note inverted δD axis.) (d) *G. bulloides* $\delta^{18}O$ record from JPC32. (e) $U^{K'}_{37}$-derived SST record. Arrow marks mean annual atlas SST at the core site [*Levitus and Boyer*, 1994]. (f) Benthic foraminiferal (*Uvigerina*) $\delta^{18}O$ record and the global benthic $\delta^{18}O$ stack of *Lisiecki and Raymo* [2005]. Shaded bar marks the early deglacial δD_{alk} decrease and associated SST cooling that coincide with Heinrich event H1.

general association of *G. oceanica* with high productivity [*Broerse et al.*, 2000; *Giraudeau*, 1992; *Martínez et al.*, 2006; *Ziveri et al.*, 1995] holds true in the Panama Basin, high glacial alkenone concentrations would suggest higher *G. oceanica* abundances and therefore lower δD_{alk} values [*Schouten et al.*, 2006], opposite to what is observed. This suggests that the last glacial D enrichment cannot be due to higher *E. huxleyi* relative to *G. oceanica* abundances, and that the observed glacial-to-interglacial δD_{alk} decline must be considered a minimum change. Furthermore, neither the early δD_{alk} decrease of ~30‰ that started at 17 ka, nor the

other millennial-scale δD_{alk} changes of the last 27 ka have obvious counterparts in the alkenone accumulation rate record (Figure 8), making it unlikely that the observed alkenone D depletions are due to transient increases of *G. oceanica* abundance relative to *E. huxleyi* abundance.

[40] Salinity changes are more difficult to evaluate through time, but most likely would act to enhance the δD_{alk} changes associated with freshwater fluxes to the ocean. *Schouten et al.* [2006] observed a positive correlation between salinity and δD_{alk} values of ~3‰/salinity unit [*Schouten et al.*, 2006], which would amplify the change
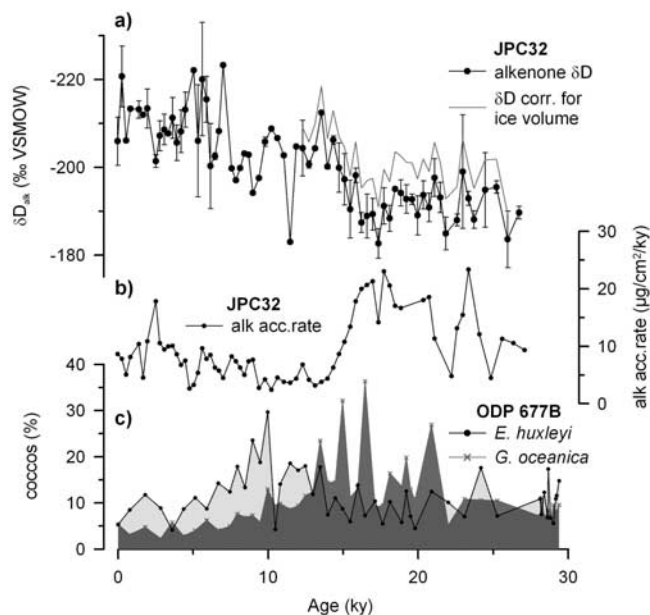
Figure 8. (a) Alkenone δD record (note inverted δD axis) and (b) alkenone accumulation rates along core JPC32 compared to (c) coccolithophorid (*E. huxleyi* and *G. oceanica*) abundances in ODP core 677B [*Martínez et al.*, 2006].

in δD_{alk} values that resulted from changes in runoff. For example, if freshwater fluxes to the Panama Basin increased, δD_{alk} values would be expected to decrease both as a result of isotopically depleted runoff and as a result of lowered salinity. Thus, in areas of strong contrast between the δD value of precipitation and seawater, and high amounts of rainfall (e.g., in the tropics close to river deltas), any changes in alkenone δD values caused by species or growth rate variations are likely to be secondary to the first-order effects caused by freshwater fluxes.

[41] The glacial alkenone D enrichment and heavy $\delta^{18}O_{plk}$ values observed in core JPC32 therefore implies reduced precipitation and runoff to the Panama Basin at that time. Relatively drier conditions can be explained by a more southern position of the ITCZ and a colder glacial atmosphere, causing hydrologic conditions similar to those encountered today during boreal winter. That is, rainfall directly associated with ITCZ convection occurring south of its present location, resulted in reduced precipitation in the Panama Basin. More importantly, the westerly, moisture-laden Chocó Jet, the primary moisture source for Colombia today that is active during boreal summer when the ITCZ is well north of the equator, must have been weaker in response to a more southern position of the ITCZ. These changes are likely to have left a substantial imprint on surface water isotopic composition, and hence δD_{alk} values in the Panama Basin.

[42] A southern mean position of the ITCZ during the last glacial maximum period relative to the Holocene is at odds with two recent studies from 8°N in the Panama Basin that suggested no LGM-Holocene change in $\delta^{18}O_{sw}$, and thus

precipitation [*Benway et al.*, 2006; *Leduc et al.*, 2007]. However, it is in agreement with both terrestrial and marine paleorecords from the tropical Atlantic and South America [e.g., *Arz et al.*, 1998; *Baker et al.*, 2001b; *Bush and Colinvaux*, 1990; *Bush*, 2002; *Hooghiemstra and van der Hammen*, 1993; *Hughen et al.*, 1996; *Leyden*, 1985; *Mora and Pratt*, 2001; *Peterson et al.*, 2000; *Schmidt et al.*, 2004; *Wang et al.*, 2004, 2006], as well as several model studies, that consistently suggest a southward shift of the ITCZ at times of high Northern Hemisphere ice volume and at times of reduced North Atlantic Deep Water (NADW) production [*Chiang and Bitz*, 2005; *Dahl et al.*, 2005; *Timmermann et al.*, 2005, 2007b]. The disparity with salinity records from ~8°N in the eastern tropical Pacific are likely due to the complexity of precipitation sources in this area. While our site and western tropical South America likely receive most of their moisture from Pacific sources, the records from 8°N lie within a second area of maximum precipitation near Costa Rica (~5°–9°N), that has been estimated to consist to 50% of Caribbean sources [*Benway and Mix*, 2004].

[43] Some Holocene δD_{alk} values in our record have large error bars because of low alkenone concentrations (see Figure 8b). Several trends, however, are apparent and robust. During the early Holocene, starting at ~9.8 ka, δD_{alk} values increased by some 12‰ and remained around −200‰ until ~8 ka, followed by a decrease of 20–25‰ until ~5 ka. The subsequent δD_{alk} increase of ~18‰ from 5–2.5 ka, suggests a drying trend that is consistent with drying in northern Venezuela [*Haug et al.*, 2001; *Tedesco and Thunell*, 2003] and a southward displacement of the ITCZ. The Cariaco Basin records indicate a minimum in precipitation around 3 ka and subsequent rapid increase that is also evident in our record as a decrease in δD_{alk} values. The long-term D depletion since 9 ka coincides with warming in the tropical Pacific (Figure 6) and is consistent with the association of warm SSTs with increased precipitation (e.g., at times of a northern mean position of the ITCZ).

5.2.2. Last Glacial Termination

[44] The last deglaciation was characterized by an early and marked SST decrease by 1.5°C from ~17 to 14.5 ka, with minimum temperatures of 23.3°C at ~15.8–15.1 ka (Figure 6). This cold event is consistent with the cooling observed in another alkenone SST record from the eastern tropical Pacific at 0°N by *Kienast et al.* [2006] (Figure 6a) and coincides with cooling and a reduction in the AMOC in the North Atlantic Ocean in response to Heinrich event H1. The simultaneity of the cold anomaly in JPC32 with H1 is supported by its occurrence during the early deglaciation, when benthic $\delta^{18}O$ in our core, and hence global ice volume, was already decreasing. Other short-duration cold episodes in the glacial section of our record may also be associated with cold events in the North Atlantic, such as the one starting around 24–23.3 ka and lasting until ~22.3 ka (Figure 6), near the time of H2. Better age control is required to confirm this association.

[45] At the time of the early deglacial cooling (H1), δD_{alk} values decreased by ~30‰ starting at ~17 ka, and reached an initial minimum at ~13.5 ka (Figure 7). As discussed above, on the basis of the alkenone accumulation record in
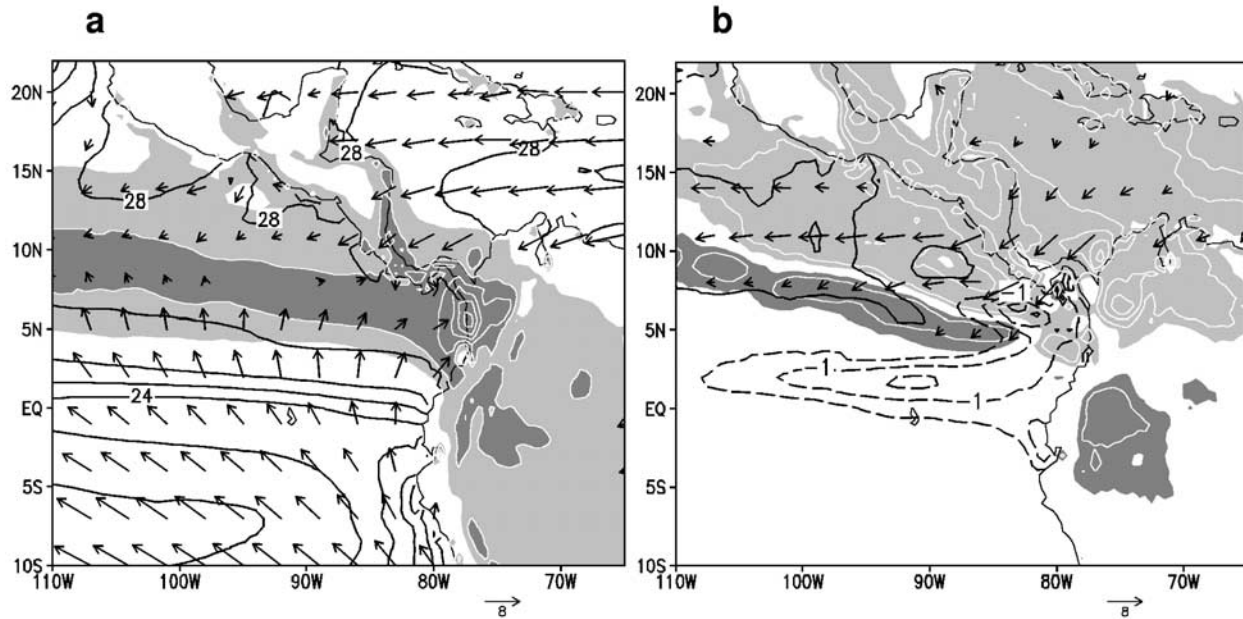
Figure 9. (a) Annual mean climatology of SST (contours at intervals of $1°C$), precipitation (white contours at intervals of 5 mm/d, light and heavy shading indicating >5 and 10 mm/d, respectively), and surface wind velocity (m/s) in the regional ocean-atmosphere model. (b) July–August–September anomalies in the "water-hosing" run: SST (black contours at $0.5°C$ intervals, with the zero contour omitted and negative values dashed), precipitation (white contours at 5 mm/d intervals, dark shading indicating >2.5 mm/d, and light shading indicating <−2.5 mm/d), and surface wind velocity (<1.5 m/s omitted for clarity). (See Appendix A for more details.)

JPC32 (Figure 8), changes in relative species abundance (*E. huxleyi* versus *G. oceanica*) are unlikely to have caused the down core δD_{alk} variations. Another factor that can potentially account for changes in surface water and hence alkenone δD independent of the amount of precipitation and runoff, are variations in moisture source. Precipitation on the Caribbean side of the Isthmus of Panama is about 30‰ more D-enriched than on the Pacific side today [*Lachniet and Patterson*, 2002; *IAEA*, 2006] and decreases by ∼30‰ in the course of cross-isthmus transport from the Atlantic to the Pacific, resulting in no significant isotopic difference of Atlantic and Pacific-derived rainfall in the eastern tropical Pacific. A change in moisture source from the Pacific to the Atlantic without a change in the amount of precipitation can therefore likely be ruled out as the cause of low and decreasing δD_{alk} values during the early deglaciation.

[46] Harsh climatic conditions characterized much of the Northern Hemisphere during H1 [*Hemming*, 2004] and the ITCZ is thought to have migrated southward [*Peterson et al.*, 2000; *Timmermann et al.*, 2005, 2007b; *Wang et al.*, 2004]. A southward displacement of the ITCZ during H1, from an already southward displaced glacial position, would have further suppressed Pacific moisture transport into tropical South America via the Chocó Jet. A concomitant δD_{alk} decrease, however, suggests the opposite, i.e., increased precipitation and runoff from Colombia.

[47] Times of high-northern latitude cooling during H events are associated with enhanced northeasterly trade winds [*Andreasen and Ravelo*, 1997; *Dahl et al.*, 2005; *Hughen et al.*, 1996] (Figure 9 and Appendix A) and

tropical to southern-subtropical Atlantic warming (including the Cariaco Basin, the Caribbean and the Gulf of Mexico [*Flower et al.*, 2004; *Hüls and Zahn*, 2000; *Rühlemann et al.*, 1999; *Schmidt et al.*, 2004; *Weldeab et al.*, 2006]). These conditions are favorable for a strengthening of low-level winds crossing Central America from the Atlantic to the Pacific (Figure 9 and Appendix A) [*Xie et al.*, 2007; *Xu et al.*, 2005]. The Panama Jet, that crosses the Isthmus of Panama from the east, develops today during boreal winter when the ITCZ is at its southernmost position and north-easterly trade winds are strongest [*Mapes et al.*, 2003; *Xie et al.*, 2005]. It accounts for part of the moisture export from the Atlantic to the Pacific that is considered crucial for the maintenance of the Atlantic-Pacific salinity difference and thus the operation of the AMOC [*Baumgartner and Reichel*, 1975; *Hostetler and Mix*, 1999; *Stocker and Wright*, 1991; *Zaucker et al.*, 1994]. The total freshwater export from the Atlantic to the Pacific across Central America through the Papagayo, Tehuantepec and Panama topographic gaps has been estimated at 0.3 Sv (1 Sv = 10^6 m^3/s) [*Stocker and Wright*, 1991] and 0.32 Sv [*Xu et al.*, 2005].

[48] An increase in moisture transport to the eastern tropical Pacific during North Atlantic H events in conjunction with cold SSTs in the Panama Basin that are documented (*Kienast et al.* [2006] and Figure 6) could have caused the increase in freshwater supply indicated by our δD_{alk} record (Figure 7). The Panama Jet leads to enhanced upwelling in the Panama Basin today [*Chelton et al.*, 2000; *Rodríguez-Rubio and Stuardo*, 2002], which should increase the impact of D-enriched subsurface waters on δD_{alk} values

while at the same time resulting in lower SSTs. Our observations from the deglaciation, however, show a cold event at ∼17 ka and low and declining δD_{alk} values relative to the LGM (Figure 7). The early deglacial δD_{alk} decrease and other short-duration δD_{alk} changes along JPC32 were therefore most likely caused by changes in freshwater supply to the Panama Basin rather than variations in upwelling.

5.3. A Regional Coupled Model Experiment

[49] In order to study the response of eastern tropical Pacific SST and precipitation to the shutdown of the AMOC during H1, we used a regional ocean-atmosphere model (ROAM) [*Xie et al.*, 2007] forced by freshening of the northern North Atlantic. This experiment simulates the cooling of the eastern tropical Pacific during H1 in consistency with paleotemperature records [*Kienast et al.*, 2006; this study, Figure 6] (see Figure 9 and see Appendix A for a more detailed description of the model). The reduction in the annual cycle of SST over the eastern equatorial Pacific in the model results from anomalous northeasterly winds across Central America (Figure 9). Moreover, the convergence of strengthened northeasterly winds across Central America in the model is associated with increased precipitation in a narrow band in the eastern tropical Pacific (Figure 9b and Appendix A). Detailed analysis of the ROAM hosing experiment indicates that this precipitation increase is due to enhanced Atlantic freshwater export across Central America during H events (I. Richter, personal communication, 2007).

[50] Our finding of increased precipitation in the eastern tropical Pacific (4.4°N) during H1 therefore appears plausible and is not in conflict with dry conditions in the Cariaco Basin [*Peterson et al.*, 2000] or at 8°N in the eastern tropical Pacific [*Benway et al.*, 2006; *Leduc et al.*, 2007].

6. Summary and Conclusions

[51] We have used hydrogen isotope ratios in alkenones, produced by haptophyte algae, to document past hydrologic changes in the Panama Basin and western tropical South America. Two records covering the past 300–400 a demonstrate that alkenone δD values reflect variations in precipitation and runoff to the tropical eastern Pacific and can be used for paleohydrologic studies. A δD_{alk} record spanning the past 27 ka indicates drier conditions during the last glacial period, likely caused by a southward shift of the ITCZ. The early deglaciation was marked by a 1.5°C sea surface cooling (∼17–14.5 ka), consistent with cooling found at 0°N in the eastern tropical Pacific [*Kienast et al.*, 2006]. This cooling coincided with the time of H1 in the North Atlantic and is consistent with the response of the eastern tropical Pacific to a reduction of the AMOC and associated strengthening of northeasterly trade winds in our ocean-atmosphere model. At the same time, a gradual δD_{alk} decrease indicates an early deglacial increase in precipitation toward Holocene conditions. Increased rainfall is supported by our model that shows a narrow band of increased precipitation in the eastern tropical Pacific in response to a reduction of the AMOC and cooling in the North Atlantic (H1). The band of increased rainfall is associated with the

convergence of anomalous northeasterly winds across Central America that are present year-round and increase the Atlantic-to-Pacific moisture transport. This may have implications for the Atlantic-Pacific freshwater balance that is critical for the operation of the AMOC.

Appendix A: Regional Coupled Model Experiment

[52] A full physics regional atmospheric model is coupled with an ocean general circulation model. The atmospheric model covers one third of the global tropics from 150°W to 30°W, 35°S to 35°N, with horizontal resolution 0.5° and 28 vertical levels. The ocean model covers the entire tropical Pacific from 35°S to 35°N, with horizontal resolution 0.5° and 30 vertical levels. The atmospheric and ocean models are restored to observations on the open boundaries, and are interactive in the eastern Pacific (east of 150°W). The ocean model west of 150°W is forced by observed atmospheric forcing while observed sea surface temperature (SST) is prescribed in the Atlantic to force the atmospheric model. The regional ocean-atmosphere model (ROAM) simulates the mean state and seasonal cycle of the eastern Pacific very well. In particular, the model reproduces the westerly Choco Jet that converges onto the Pacific coast of Colombia and creates a rainfall maximum exceeding 10 m/a (Figure 9a). For a detailed description of the model and its performance, readers are referred to *Xie et al.* [2007].

[53] In response to an injection of fresh water in the high-latitude North Atlantic, as at the onset of Heinrich events, the cooling of the tropical North Atlantic is a common feature in different coupled general circulation models (GCMs) [*Timmermann et al.*, 2007b]. The ROAM is used to investigate how this North Atlantic cooling induces changes in the tropical Pacific via the mountainous Central American Isthmus. Tropical North Atlantic SST is reduced by 2°C to mimic the response there to water hosing. The prescribed cooling is spatially uniform north of 5°N and tempered down to zero to 5°S. The cooling causes atmospheric pressure to increase over the tropical North Atlantic and the increased pressure gradient with the Pacific drives anomalous northeasterly winds across Central America, a feature seen in all coupled GCMs in response to North Atlantic water hosing [*Timmermann et al.*, 2007b]. The anomalous northeasterly winds across Central America cause a reduction in the SST annual cycle over the equatorial eastern Pacific [*Xie et al.*, 2007].

[54] Figure 9b shows the model response to North Atlantic cooling during July–August–September (JAS), the season when the atmospheric changes in wind and precipitation are the most pronounced since tropical North Atlantic SST is at its annual maximum and supports deep atmospheric convection. As a result, a unit change in SST there can induce a larger atmospheric response during JAS than in other seasons. Strong northeasterly wind anomalies of up to 8 m/s are found across Central America and cover a broad region over the eastern Pacific north of the equator. Negative SST anomalies are found on the coast from Panama to Ecuador, consistent with Alkenone SST observations during the Heinrich event [*Kienast et al.*, 2006; this

study]. Precipitation decreases over much of the northeastern tropical Pacific, in line with paleosalinity reconstructions from this area [*Benway et al.*, 2006; *Leduc et al.*, 2007]. However, there is a narrow ribbon of increased rainfall to the south. This ribbon of increased rainfall is associated with the convergence of anomalous northeasterly winds across Central America and appears to be consistent with an intensified hydrological cycle during the Heinrich event as inferred from our δD_{alk} record at JPC32. The anomalous cross–Central American winds are present year-round and increase the Atlantic-to-Pacific transport of moisture.

References

Andreasen, D. J., and A. C. Ravelo (1997), Tropical Pacific Ocean thermocline depth reconstructions for the last glacial maximum, *Paleoceanography*, *12*(3), 395–414.

Arz, H. W., et al. (1998), Correlated millennial-scale changes in surface hydrography and terrigenous sediment yield inferred from last-glacial marine deposits off northeastern Brazil, *Quat. Res.*, *50*(2), 157–166.

Baker, P. A., et al. (2001a), Tropical climate changes at millennial and orbital timescales on the Bolivian Altiplano, *Nature*, *409*, 698–701.

Baker, P. A., et al. (2001b), The history of South American tropical precipitation for the past 25,000 years, *Science*, *291*, 640–643.

Baumgartner, A., and E. Reichel (1975), *The World Water Balance*, 179 pp., Elsevier, New York.

Benway, H. M., and A. C. Mix (2004), Oxygen isotopes, upper-ocean salinity, and precipitation sources in the eastern tropical Pacific, *Earth Planet. Sci. Lett.*, *224*, 493–507.

Benway, H. M., A. C. Mix, B. A. Haley, and G. P. Klinkhammer (2006), Eastern Pacific Warm Pool paleosalinity and climate variability: 0–30 kyr, *Paleoceanography*, *21*, PA3008, doi:10.1029/2005PA001208.

Broerse, A. T. C., et al. (2000), Coccolithophore export production in response to monsoonal upwelling off Somalia (northwestern Indian Ocean), *Deep Sea Res., Part II*, *47*(9–11), 2179–2205.

Burgoyne, T. W., and J. M. Hayes (1998), Quantitative production of H$_2$ by pyrolysis of gas chromatographic effluents, *Anal. Chem.*, *70*(24), 5136–5141.

Bush, M. B. (2002), On the interpretation of fossil Poaceae pollen in the lowland humid neotropics, *Palaeogeogr. Palaeoclimatol. Palaeoecol.*, *177*(1–2), 5–17.

Bush, M. B., and P. A. Colinvaux (1990), A pollen record of a complete glacial cycle from lowland Panama, *J. Veg. Sci.*, *1*(1), 105–118.

Bush, M. B., et al. (1992), A 14,300-yr paleoecological profile of a lowland tropical lake in Panama, *Ecol. Monogr.*, *62*(2), 251–275.

Bush, M. B., et al. (2002), Orbital forcing signal in sediments of two Amazonian lakes, *J. Paleolimnol.*, *27*(3), 341–352.

Chelton, D. B., et al. (2000), Satellite observations of the wind jets off the Pacific coast of Central America. part II: Regional relationships and dynamical considerations, *Mon. Weather Rev.*, *128*(7), 2019–2043.

Chiang, J. C. H. (2005), Present-day climate variability in the tropical Atlantic: A model for paleoclimate changes?, in *The Hadley Circulation: Past, Present, and Future*, edited by H. F. Diaz and R. S. Bradley, pp. 465–488, Kluwer Acad., Dordrecht, Netherlands.

Chiang, J. C. H., and C. M. Bitz (2005), Influence of high latitude ice cover on the marine Intertropical Convergence Zone, *Clim. Dyn.*, *25*, 477–496.

Colinvaux, P. A., et al. (1996), A long pollen record from lowland Amazonia: Forest and cooling in glacial times, *Science*, *274*, 85–88.

Conte, M. H., M.-A. Sicre, C. Rühlemann, J. C. Weber, S. Schulte, D. Schulz-Bull, and T. Blanz (2006), Global temperature calibration of the alkenone unsaturation index (U$^{K'}_{37}$) in surface waters and comparison with surface sediments, *Geochem. Geophys. Geosyst.*, *7*, Q02005, doi:10.1029/2005GC001054.

Cruz, F. W., et al. (2005), Insolation-driven changes in atmospheric circulation over the past 116,000 years in subtropical Brazil, *Nature*, *434*, 63–66.

Dahl, K., et al. (2005), Assessing the role of North Atlantic freshwater forcing in millennial scale climate variability: A tropical Atlantic perspective, *Clim. Dyn.*, *24*, 325–346.

Dansgaard, W. (1964), Stable isotopes in precipitation, *Tellus*, *16*, 436–468.

Duplessy, J. C., et al. (1991), Surface salinity reconstruction of the North Atlantic Ocean during the last glacial maximum, *Oceanol. Acta*, *14*(4), 311–324.

Englebrecht, A. C., and J. P. Sachs (2005), Determination of sediment provenance at drift sites using hydrogen isotopes and unsaturation ratios in alkenones, *Geochim. Cosmochim. Acta*, *69*(17), 4253–4265.

Flower, B. P., et al. (2004), Phasing of deglacial warming and Laurentide ice sheet meltwater in the Gulf of Mexico, *Geology*, *32*(7), 597–600.

Gat, J. R. (1996), Oxygen and hydrogen isotopes in the hydrologic cycle, *Annu. Rev. Earth Planet. Sci.*, *24*, 225–262.

Giraudeau, J. (1992), Distribution of Recent nannofossils beneath the Benguela system: Southwest African continental margin, *Mar. Geol.*, *108*(2), 219–237.

Goldberg, E. D. (1963), Geochronology with ^{210}Pb, in *Proceedings of the Symposium on Radioactive Dating*, pp. 121–131, Int. At. Energy Agency, Vienna.

Gonfiantini, R., et al. (2001), The altitude effect on the isotopic composition of tropical rains, *Chem. Geol.*, *181*(1–4), 147–167.

Hall, A., and S. Manabe (2000), Effect of water vapor feedback on internal and anthropogenic variations of the global hydrologic cycle, *J. Geophys. Res.*, *105*(D5), 6935–6944.

Haug, G. H., et al. (2001), Southward migration of the Intertropical Convergence Zone through the Holocene, *Science*, *293*, 1304–1308.

Hemming, S. R. (2004), Heinrich events: Massive late Pleistocene detritus layers of the North Atlantic and their global climate imprint, *Rev. Geophys.*, *42*, RG1005, doi:10.1029/2003RG000128.

Hooghiemstra, H., and T. van der Hammen (1993), Late Quaternary vegetation history and paleoecology of Laguna Pedro Palo (subandean forest belt, Eastern Cordillera, Colombia), *Rev. Palaeobot. Palynol.*, *77*(3–4), 235–262.

Hostetler, S. W., and A. C. Mix (1999), Reassessment of ice-age cooling of the tropical ocean and atmosphere, *Nature*, *399*, 673–676.

Hughen, K. A., et al. (1996), Rapid climate changes in the tropical Atlantic region during the last deglaciation, *Nature*, *380*, 51–54.

Hüls, M., and R. Zahn (2000), Millennial-scale sea surface temperature variability in the western tropical North Atlantic from planktonic foraminiferal census counts, *Paleoceanography*, *15*(6), 659–678.

Kienast, M., et al. (2001), Synchronous tropical South China Sea SST change and Greenland warming during deglaciation, *Science*, *291*, 2132–2134.

Kienast, M., et al. (2006), Eastern Pacific cooling and Atlantic overturning circulation during the last deglaciation, *Nature*, *443*, 846–849.

Koutavas, A., and J. Lynch-Stieglitz (2003), Glacial-interglacial dynamics of the eastern equatorial Pacific cold tongue-Intertropical Convergence Zone system reconstructed from oxygen isotope records, *Paleoceanography*, *18*(4), 1089, doi:10.1029/2003PA000894.

Koutavas, A., et al. (2002), El Niño-like pattern in ice age tropical Pacific sea surface temperature, *Science*, *297*, 226–230.

Koutavas, A., et al. (2004), Holocene sea surface temperature trends in the equatorial Pacific Ocean, paper presented at 1st International CLIVAR Conference, CLIVAR, Baltimore, Md.

Krebs, U., and A. Timmermann (2007), Tropical air-sea interactions accelerate the recovery of the Atlantic meridional overturning circulation after a major shutdown, *J. Clim.*, *20*(19), 4940–4956.

Krishnaswamy, S., et al. (1971), Geochronology of lake sediments, *Earth Planet. Sci. Lett.*, *11*, 407–414.

Lachniet, M. S., and W. P. Patterson (2002), Stable isotope values of Costa Rican surface waters, *J. Hydrol.*, *260*(1–4), 135–150.

Lea, D. W., et al. (2000), Climate impact of late Quaternary equatorial Pacific sea surface temperature variations, *Science*, 289, 1719–1724.

Leduc, G., et al. (2007), Moisture transport across Central America as a positive feedback on abrupt climatic changes, *Nature*, 445, 908–911.

Levitus, S., and T. P. Boyer (1994), *World Ocean Atlas 1994*, vol. 4, *Temperature*, NOAA Atlas NESDIS, vol. 4, NOAA, Silver Spring, Md..

Levitus, S., et al. (1994), *World Ocean Atlas 1994*, vol. 3, *Salinity*, NOAA Atlas NESDIS, vol. 3, NOAA, Silver Spring, Md.

Leyden, B. W. (1985), Late Quaternary aridity and Holocene moisture fluctuations in the Lake Valencia Basin, Venezuela, *Ecology*, 66(4), 1279–1295.

Lisiecki, L. E., and M. E. Raymo (2005), A Pliocene-Pleistocene stack of 57 globally distributed benthic $\delta^{18}O$ records, *Paleoceanography*, 20, PA1003, doi:10.1029/2004PA001071.

Mapes, B. E., et al. (2003), Diurnal patterns of rainfall in northwestern South America. part I: Observations and context, *Mon. Weather Rev.*, 131(5), 799–812.

Martínez, J., et al. (2006), Foraminifera and coccolithophorid assemblage changes in the Panama Basin during the last deglaciation: Response to sea-surface productivity induced by a transient climate change, *Palaeogeogr. Palaeoclimatol. Palaeoecol.*, 234(1), 114–126.

Maslin, M. A., and S. J. Burns (2000), Reconstruction of the Amazon Basin effective moisture availability over the past 14,000 years, *Science*, 290, 2285–2287.

Mayle, F. E., et al. (2004), Responses of Amazonian ecosystems to climatic and atmospheric carbon dioxide changes since the last glacial maximum, *Philos. Trans. R. Soc. London, Ser. B*, 359(1443), 499–514.

Mora, G., and L. M. Pratt (2001), Isotopic evidence for cooler and drier conditions in the tropical Andes during the last glacial stage, *Geology*, 29(6), 519–522.

Müller, P. J., et al. (1998), Calibration of the alkenone paleotemperature index $U_{37}^{K'}$ based on core-tops from the eastern South Atlantic and the global ocean (60°N–60°S), *Geochim. Cosmochim. Acta*, 62(10), 1757–1772.

Pahnke, K., and J. P. Sachs (2006), Sea surface temperatures of southern midlatitudes 0–160 kyr B. P., *Paleoceanography*, 21, PA2003, doi:10.1029/2005PA001191.

Paul, H. A. (2002), Application of novel stable isotope methods to reconstruct paleoenvironments: Compound-specific hydrogen isotopes and pore-water oxygen isotopes, Ph.D. thesis, ETH Zurich, Zurich, Switzerland.

Peterson, L. C., and G. H. Haug (2006), Variability in the mean latitude of the Atlantic Intertropical Convergence Zone as recorded by riverine input of sediments to the Cariaco Basin (Venezuela), *Palaeogeogr. Palaeoclimatol. Palaeoecol.*, 234(1), 97–113.

Peterson, L. C., et al. (2000), Rapid changes in the hydrologic cycle of the tropical Atlantic during the last glacial, *Science*, 290, 1947–1951.

Poveda, G., and O. J. Mesa (1997), Feedbacks between hydrological processes in tropical South America and large-scale ocean-atmospheric phenomena, *J. Clim.*, 10(10), 2690–2702.

Poveda, G., and O. J. Mesa (2000), On the existence of Lloro (the rainiest locality on Earth): Enhanced ocean-land-atmosphere interaction by a low-level jet, *Geophys. Res. Lett.*, 27(11), 1675–1678.

Poveda, G., et al. (2001), Seasonality in ENSO–related precipitation, river discharges, soil moisture, and vegetation index in Colombia, *Water Resour. Res.*, 37(8), 2169–2178.

Prahl, F. G., et al. (1988), Further evaluation of long-chain alkenones as indicators of paleoceanographic conditions, *Geochim. Cosmochim. Acta*, 52(9), 2303–2310.

Prahl, F. G., et al. (2005), Ecology and biogeochemistry of alkenone production at station ALOHA, *Deep Sea Res., Part I*, 52(5), 699–719.

Ramaswamy, V., and Members of IPCC Working Group I (2001), *Radiative Forcing of Climate Change*, Cambridge Univ. Press, New York.

Restrepo, J. D., and B. Kjerfve (2000), Water discharge and sediment load from the western slopes of the Colombian Andes with focus on Rio San Juan, *J. Geol.*, 108, 17–33.

Restrepo, J. D., and B. Kjerfve (2002), The San Juan Delta, Colombia: Tides, circulations, and salt dispersion, *Cont. Shelf Res.*, 22(8), 1249–1267.

Rodríguez-Rubio, E., and J. Stuardo (2002), Variability of photosynthetic pigments in the Colombian Pacific Ocean and its relationship with the wind field using ADEOS-I data, *Proc. Indian Acad. Sci. Earth Planet. Sci.*, 11(3), 227–236.

Rodríguez-Rubio, E., W. Schneider, and R. Abarca del Río (2003), On the seasonal circulation within the Panama Bight derived from satellite observations of wind, altimetry and sea surface temperature, *Geophys. Res. Lett.*, 30(7), 1410, doi:10.1029/2002GL016794.

Rozanski, K., et al. (1992), Relation between long-term trends of oxygen-18 isotope composition of precipitation and climate, *Science*, 258, 981–985.

Rozanski, K. L. Araguás-Araguás, and R. Gonfiantini (1993), Isotopic patterns in modern global precipitation, in *Climate Change in Continental Isotopic Records*, Geophys. Monogr. Ser., vol. 78, edited by P. K. Swart et al., pp. 1–36, AGU, Washington, D. C.

Rühlemann, C., et al. (1999), Warming of the tropical Atlantic Ocean and slowdown of thermohaline circulation during the last deglaciation, *Nature*, 402, 511–514.

Sachse, D., et al. (2004), Hydrogen isotope ratios of recent lacustrine sedimentary n-alkanes record modern climate variability, *Geochim. Cosmochim. Acta*, 68(23), 4877–4889.

Sachse, D., et al. (2006), δD values of individual n-alkanes from terrestrial plants along a climatic gradient—Implications for the sedimentary biomarker record, *Org. Geochem.*, 37(4), 469–483.

Sauer, P. E., et al. (2001), Compound-specific D/H ratios of lipid biomarkers from sediments as a proxy for environmental and climatic conditions, *Geochim. Cosmochim. Acta*, 65(2), 213–222.

Schmidt, M. W., et al. (2004), Links between salinity variation in the Caribbean and North Atlantic thermohaline circulation, *Nature*, 428, 160–163.

Schouten, S., et al. (2006), The effect of temperature, salinity and growth rate on the stable hydrogen isotopic composition of long chain alkenones produced by *Emiliania huxleyi* and *Gephyrocapsa oceanica*, *Biogeosciences*, 3, 113–119.

Schrag, D. P., et al. (2002), The oxygen isotopic composition of seawater during the Last Glacial Maximum, *Quat. Sci. Rev.*, 21, 331–342.

Sessions, A. L., et al. (1999), Fractionation of hydrogen isotopes in lipid biosynthesis, *Org. Geochem.*, 30(9), 1193–1200.

Sessions, A. L., et al. (2001), Correction of H_3^+ contributions in hydrogen isotope ratio monitoring mass spectrometry, *Anal. Chem.*, 73(2), 192–199.

Sessions, A. L., et al. (2004), Isotopic exchange of carbon-bound hydrogen over geologic timescales, *Geochim. Cosmochim. Acta*, 68(7), 1545–1559.

Small, R. J. O., et al. (2007), The Central American mid-summer drought: Regional aspects and large scale forcing, *J. Clim.*, 20(19), 4853–4873.

Stocker, T. F., and S. J. Johnsen (2003), A minimum thermodynamic model for the bipolar seesaw, *Paleoceanography*, 18(4), 1087, doi:10.1029/2003PA000920.

Stocker, T. F., and D. G. Wright (1991), Rapid transitions of the ocean's deep circulation induced by changes in surface water fluxes, *Nature*, 351, 729–732.

Stott, L., et al. (2004), Decline of surface temperature and salinity in the western tropical Pacific Ocean in the Holocene epoch, *Nature*, 431, 56–59.

Stott, L. D., et al. (2002), Super ENSO and global climate oscillations at millennial time scales, *Science*, 297, 222–226.

Stouffer, R. J., et al. (2007), Climate response to external sources of freshwater: North Atlantic versus the Southern Ocean, *J. Clim.*, 20(3), 436–448.

Stute, M., et al. (1995), A 30,000 yr continental paleotemperature record derived from noble gases dissolved in groundwater from the San Juan Basin, New Mexico, *Quat. Res.*, 43(2), 209–220.

Tedesco, K., and R. Thunell (2003), High resolution tropical climate record for the last 6,000 years, *Geophys. Res. Lett.*, 30(17), 1891, doi:10.1029/2003GL017959.

Timmermann, A., et al. (2004), Surface temperature control in the North and tropical Pacific during the last glacial maximum, *Clim. Dyn.*, 23, 353–370.

Timmermann, A., U. Krebs, F. Justino, H. Goosse, and T. Ivanochko (2005), Mechanisms for millennial-scale global synchronization during the last glacial period, *Paleoceanography*, 20, PA4008, doi:10.1029/2004PA001090.

Timmermann, A., et al. (2007a), The effect of orbital forcing on the mean climate and variability of the tropical Pacific, *J. Clim.*, 20(16), 4147–4159.

Timmermann, A., et al. (2007b), The influence of a weakening of the Atlantic meridional overturning circulation on ENSO, *J. Clim.*, 20(19), 4899–4919.

Turner, L. J., and L. D. Delorme (1996), Assessment of ^{210}Pb data from Canadian lakes using the CIC and CRS models, *Environ. Geol.*, 28(2), 78–87.

Turney, C. S. M., et al. (2004), Millennial and orbital variations of El Niño/Southern Oscillation and high-latitude climate in the last glacial period, *Nature*, 428, 306–310.

Vernekar, A. D., et al. (2003), Low-level jets and their effects on the South American summer climate as simulated by the NCEP Eta model, *J. Clim.*, 16(2), 297–311.

Waelbroeck, C., et al. (2002), Sea-level and deep water temperature changes derived from benthic foraminifera isotopic records, *Quat. Sci. Rev.*, 21, 295–305.

Wang, X., et al. (2004), Wet periods in northeastern Brazil over the past 210 kyr linked to

distant climate anomalies, *Nature*, *432*, 740–743.

Wang, X., et al. (2006), Interhemispheric antiphasing of rainfall during the last glacial period, *Quat. Sci. Rev.*, *25*, 3391–3403.

Weldeab, S., et al. (2006), Deglacial sea surface temperature and salinity increase in the western tropical Atlantic in synchrony with high latitude climate instabilities, *Earth Planet. Sci. Lett.*, *241*(3–4), 699–706.

Xie, S.-P., and J. A. Carton (2004), Tropical Atlantic variability: Patterns, mechanisms, and impacts, in *Earth's Climate: The Ocean-Atmosphere Interaction*, *Geophys, Monogr. Ser.*, vol. 147, edited by C. Wang, S.-P. Xie, and J. A. Carton, pp. 121–142, AGU, Washington, D. C.

Xie, S.-P., et al. (2005), Air-sea interaction over the eastern Pacific warm pool: Gap winds, thermocline dome, and atmospheric convection, *J. Clim.*, *18*(1), 5–20.

Xie, S.-P., et al. (2007), A regional ocean-atmosphere model for eastern Pacific climate: To-

ward reducing tropical biases, *J. Clim.*, *20*(8), 1504–1522.

Xu, H., et al. (2005), Effects of Central American mountains on the eastern Pacific winter ITCZ and moisture transport, *J. Clim.*, *18*(18), 3856–3873.

Yakir, D., and M. J. DeNiro (1990), Oxygen and hydrogen isotope fractionation during cellulose metabolism in *Lemna gibba L*, *Plant Physiol.*, *93*, 325–332.

Zaucker, F., T. F. Stocker, and W. S. Broecker (1994), Atmospheric freshwater fluxes and their effect on the global thermohaline circulation, *J. Geophys. Res.*, *99*(C6), 12,443–12,458.

Zhang, R., and T. L. Delworth (2005), Simulated tropical response to a substantial weakening of the Atlantic thermohaline circulation, *J. Clim.*, *18*(12), 1853–1860.

Zhang, Z., and J. P. Sachs (2007), Hydrogen isotope fractionation in freshwater algae: I. Variations among lipids and species, *Org. Geochem.*, *38*(4), 582–608.

Ziveri, P., et al. (1995), Export production of coccolithophores in an upwelling region: Results from San Pedro Basin, southern California borderlands, *Mar. Micropaleontol.*, *24*(3–4), 335–358.

————————————

L. Keigwin, Woods Hole Oceanographic Institution, Woods Hole, MA 02543, USA.

K. Pahnke, Department of Geochemistry, Lamont-Doherty Earth Observatory, Earth Institute at Columbia University, 61 Route 9 W, Palisades, NY 10964, USA. (kpahnke@ldeo.columbia.edu)

J. P. Sachs, School of Oceanography, University of Washington, Seattle, WA 98195, USA. (jsachs@u.washington.edu)

A. Timmermann and S.-P. Xie, International Pacific Research Center, SOEST, University of Hawaii at Manoa, Honolulu, HI 96822, USA.